



# New Interferometric Imaging Methods: Parsimonious Interferometry and Supervirtual Interferometry+Tomography for Far-Offset Refractions

Jing Li, Kai Lu, Sherif Hanafy, and Gerard Schuster\* (gerard.schuster@kaust.edu.sa)

Copyright 2017, SBGf - Sociedade Brasileira de Geofísica

This paper was prepared for presentation during the 15<sup>th</sup> International Congress of the Brazilian Geophysical Society held in Rio de Janeiro, Brazil, 31 July to 3 August, 2017.

Contents of this paper were reviewed by the Technical Committee of the 15<sup>th</sup> International Congress of the Brazilian Geophysical Society and do not necessarily represent any position of the SBGf, its officers or members. Electronic reproduction or storage of any part of this paper for commercial purposes without the written consent of the Brazilian Geophysical Society is prohibited.

Two new interferometric imaging methods are presented: parsimonious interferometry (PI) for fast acquisition of refraction surveys and supervirtual refraction interferometry (SVI) for enhancing the signal-to-noise ratio of far-offset refractions. The far-offset traveltimes are inverted by traveltime tomography to give the deep portions of the velocity model. We demonstrate the benefits and liabilities of these methods with synthetic data and field data examples.

## Introduction

We will introduce two novel imaging technologies: PI and SVI.

### Parsimonious Interferometry:

Assume two reciprocal sources and the checkerboard layered medium in Figure 1, where head waves propagate along the interface between the upper and lower layers. There can be lateral velocity variations in the upper medium and there are N evenly spaced geophones on the recording surface between the two sources. The head-wave traveltime from the source at A to the geophone at C is given by

$$T_{AC} = T_{Ax'} + T_{x'x} + T_{xC}, \quad (1)$$

and the reciprocal traveltime from D to B is

$$T_{DB} = T_{Dx} + T_{x'x} + T_{x'B}, \quad (2)$$

where  $T_{xx}$  is the traveltime from x to x' along the refraction ray. Reciprocity demands that  $T_{xx} = T_{x'x}$ . To create virtual sources and receivers within the array, we define the stationary interferometric condition for the postcritical geophone locations C and B between the reciprocal sources at A and D:

$$|C - A| + |B - D| > |A - D|, \quad (3)$$

which means that C is to the right of B. We also demand that C and B are separated by a critical offset where a refraction arrival would be recorded at B if a source was placed at C. Subtracting the reciprocal traveltime  $T_{AD} = T_{Ax'} + T_{x'x} + T_{xD}$  from the sum  $T_{AC} + T_{DB}$  gives the stationary interferometric traveltime  $\delta T_{CB}$ :

$$\begin{aligned} \delta T_{CB} &= T_{AC} + T_{DB} - T_{AD}, \\ &= T_{Ax'} + T_{x'x} + T_{xC} + [T_{Dx} + T_{x'x'} + T_{x'B}] - T_{Ax'} - T_{x'x} - T_{xD}, \\ &= T_{Cx} + T_{x'x'} + T_{x'B}, \end{aligned} \quad (4)$$

where B is at a postcritical distance to the left of C.  $\delta T_{CB}$  is denoted as an interferometric stationary traveltime because the reciprocal raypath  $Ax'xD$ , marked by the dashed red ray in Figure 1, cancels the phase associated with the common raypaths of the purple  $Ax'xC$  and green  $Dxx'B$  rays. The result is the virtual traveltime  $\delta T_{CB}$  associated with the much shorter raypath  $Cxx'B$  denoted by the dashed blue ray. Thus,  $\delta T_{CB}$  is associated with a virtual source at C exciting a virtual refraction arrival that is recorded at B. This natural redatuming operation is the key principle underlying seismic interferometry (Schuster, 2009).

Equation 4 satisfies Fermat's interferometric principle because the subtraction of  $T_{AD}$  (red dashed ray) from  $T_{AC} + T_{AB}$  (solid green and purple rays) gives the same value of  $\delta T_{CB}$  for all postcritical, i.e. stationary, locations of the reciprocal sources.

Therefore, equation 4 can be used to generate  $O(N)$  virtual shot gathers, where the number of reciprocal geophone pairs that satisfy the stationary interferometric condition in equation 3 is assumed to be nearly equal to the number N of geophones in the survey. Each virtual shot gather will, on average, contain  $O(N/2)$  virtual traveltimes generated by equation 4. This means that parsimonious interferometry can create  $O(N^2)/2$  virtual refraction traveltimes from the  $2N$  traveltimes picked from two reciprocal shot gathers. This abundance of new traveltimes can be used to invert for the subsurface velocity model with much greater ray density and better model resolution than inverted from the original data set. The above analysis assumed only one refractor, but it can be extended to models with multiple refractors.

**Supervirtual Refraction Interferometry:** Far-offset first arrivals are often polluted with noise so their arrival times cannot be reliably picked and inverted for the subsurface velocity model. To overcome this problem, Mallinson et al. (2011) developed the theory of supervirtual refraction interferometry to create head-wave arrivals with much improved SNRs. They demonstrated the efficacy of this with both synthetic data and field data. Their examples were restricted to 2D velocity models and 2D survey lines, but recent work by Lu and Schuster (2014) show that SVI can also be extended to data recorded by 3D surveys. We will now show field data results that extend the usable offset of traces from about 10 km to 18 km for a 3D marine data with OBS recorders.

## Theory and Practice

We will introduce the theories and workflows for PI and SVI. Each description will be accompanied by results using both synthetic seismograms and field data.

**Theory of PI:** The implementation of PI for refraction waves are presented in Hanafy and Schuster (2017), and the workflow for PI is described below.

1. Collect two reciprocal shot gathers, where there is a source at each end of the geophone line. The  $2N$  refraction traveltimes are picked and equation 4 is used to transform them into  $O(N^2)$  virtual refraction traveltimes.
2. Invert the refraction traveltimes by ray-based tomography or wave equation traveltime inversion (Hanafy and Schuster, 2017).

**PI Numerical Results:** The two-layer model is shown in Figure 2a and a finite-difference solution to the eikonal equation is used to compute 120 shot gathers of first-arrival traveltimes, with a source located every 5 m. The geophones are placed every 5 meters on the surface. The 240 first-arrival traveltimes from the two reciprocal shot gathers, where one source is at (0, 0) and the other is at (0, 600 m), were then inverted by traveltime tomography to get the reciprocal tomogram in Figure 2b. In this case there is a poor correspondence between the reciprocal tomogram and the actual velocity model. For comparison, Figure 2c shows the standard tomogram inverted from 14,400 actual traveltimes generated by placing shots at each of the 120 geophones. As expected, the standard tomogram mostly agrees with the actual velocity model.

Equation 4 is then used to compute the virtual traveltimes from the 240 traveltimes associated with the two reciprocal shot gathers. The result is the creation of  $O(14,000)$  virtual traveltimes computed for virtual shots at each of the geophones. These virtual traveltimes agree with the actual ones to within a maximum error of less than 0.1 ms, and the virtual tomogram is shown in Figure 2d. As expected, there is a close correspondence between the standard and virtual tomograms.

The PI method is also tested for the complicated Aqaba model in Figure 3a. In this case the virtual tomogram in Figure 3d closely resembles the standard tomogram in Figure 3c. In contrast, the reciprocal tomogram in Figure 3b is far from the true model.

The parsimonious procedure can also be applied to surface waves, except the traces in the two reciprocal shot gathers are correlated with one another to get virtual surface wave records with virtual shots located at each geophone. The Rayleigh waves in these virtual shot gathers can then be inverted (Li and Schuster, 2017) to give the S-velocity tomograms shown in Figure 4. In this case two reciprocal shot gathers were used to generate  $70^2$  virtual shot gathers, and these were inverted to track the percolation of the water into the soil.

A reciprocal survey, with 70 geophones along a 60 m line, was carried every 5 minutes, with a shot at each end of the geophone line, and two infill shot gathers. After

correlating trace pairs, we generate about  $70^2$  virtual shot gathers with about 70 traces per shot gather. The surface waves are inverted using the wave equation dispersion inversion method of Li et al. (2017). The tomograms above are the differences between the background S-velocity model and the velocity models obtained by inverting the surface waves in the different reciprocal surveys.

**Theory of SVI:** The theory of supervirtual interferometry is presented in Bharadwaj et al. (2011), and is described by the workflow in Figure 5. There are two steps to SVI: identify receiver pairs at **A** and **B** in Figure 5a where the first arrival generated by the source at **x** is a head wave from the same refractor. Correlate the traces at **A** and **B** with one another to give the correlogram  $\Phi_x(\mathbf{A}, \mathbf{B}, t)$  associated with the ray diagram on the right of Figure 5a. The arrival time of the event in  $\Phi_x(\mathbf{A}, \mathbf{B}, t)$  will be identical to those from first arrivals generated by a post-critical source at **x**, as long as the first arrival is from the same refracting interface. Therefore, stacking the correlograms  $\Sigma_x \Phi_x(\mathbf{A}, \mathbf{B}, t)$  over different post-critical source positions enhances the SNR by  $\sqrt{N}$ . Similar considerations show that convolving the correlograms with actual traces and stacking the result will further enhance the SNR as illustrated in Figures 5b and 5c. The major benefit of SVI is that it typically resurrects noisy traces at the far-offset positions so that the first-arrival traveltimes can be accurately picked.

The liability of SVI is that it assumes that the first-arrivals are largely those for head waves. However, experience with synthetic data and field data examples suggest that SVI is largely robust even in the presence of diving waves as first arrivals.

**SVI Numerical Results:** The SVI method is tested on synthetic CSGs computed for a 3D undulating two-layer model with the upper and lower P-velocities of 1500 m/s and 3000 m/s, respectively. The acquisition geometry has 11 survey lines on the surface, with 76 shots and 301 receivers in each line. The shots are spaced every 80 m, the receivers are at 20 m intervals and the line spacing is 100 m.

A common shot gather is shown in Figure 6a, where the maximum source-receiver offset is more than 3 km. The first arrivals in the far-offset traces are impossible to pick after strong random noise is added to give the CSG in Figure 6b. 3D SVI (Lu et al., 2014) is applied to these noisy data to give the super-virtual data shown in Figure 6c. Compared to the input shown in Figure 6b, the SVI CSG in Figure 6c has the correct traveltimes and a much improved SNR. Figure 6d shows the result after 2 iterations of SVI (Al-Hagan et al., 2014) are applied to these data, so that the SNR is further enhanced compared to Figure 6c. Now, the traveltimes of the far-offset refractions can be accurately picked and inverted to image the velocity in the deep portions of the model. The phase distortion due to correlation and convolution of the traces can easily be corrected by comparison to a recorded trace with a first-arrival that has a high SNR.

A marine experiment with OBS receivers is conducted to give a 3D data set. The first-arrival traveltimes are pickable out to a source-receiver offset of about 10 km, and after that the first arrivals are too noisy to be accurately picked. Figure 7 shows the a) filtered and b) SVI traces at the far offset geophone positions. It is clear that SVI has significantly enhanced the far-offset first-arrivals so their traveltimes can be accurately picked and inverted.

## Conclusions

Seismic data recorded in rugged foothill environments require rugged imaging methods that will withstand the challenges of low SNR and rugged topography. SVI applied to noisy far-offset records will allow for accurate traveltimes picking of first arrivals. Such traveltimes can be inverted by traveltimes tomography to get P-velocity information about the deep portions of a basin. To reduce acquisition time we can perform parsimonious interferometry and transform two reciprocal shot gathers into  $N^2$  shot gathers, where  $N$  is the number of geophones. The refraction traveltimes and the surface waves can be inverted to give the subsurface P-velocity and S-velocity models, respectively. The liability of parsimonious refraction interferometry is that it implicitly assumes that the refraction arrival is that of a head wave. This might not be true for strong vertical gradients in the velocity model.

## References

- Al-Hagan, S. Hanafy, and G. Schuster, 2014, Iterative supervirtual refraction interferometry: *Geophysics*, **79**, Q21-Q30.
- Bharadwaj, P., G. T. Schuster, and I. Mallinson, 2011, Theory of supervirtual refraction interferometry: *Geo. J. Int.*, **288**, 263–273.
- Hanafy, S. and G.T. Schuster, 2017, Parsimonious refraction interferometry and tomography: *Geophys. J. Int.*, DOI: 10.1093/gji/ggx042.
- Li, J., S. Hanafy, and G. Schuster, 2017, Wave equation dispersion inversion: *Geophys. J. Int.*, doi: 10.1093/gji/ggw465.
- Li, J. and G.T. Schuster, 2017, Parsimonious surface-wave interferometry: *Geophys. J. Internat.* (submitted).
- Lu, K., A. AlTheyab, and G. T. Schuster, 2014, 3D supervirtual refraction interferometry: *SEG Technical Program Expanded Abstracts*, 4203-4207.
- Luo, Y., and G. T. Schuster, 1991, Wave equation inversion of skeletalized geophysical data: *Geo. J. Int.*, **105**, 289–294.
- Schuster, G., 2009, *Seismic Interferometry*: Cambridge Press.

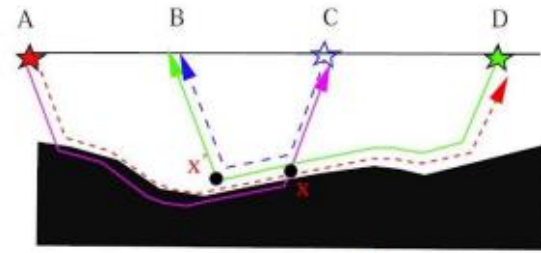


Figure 1: Two-layer model where the black medium is faster than the top layer; the reciprocal sources are at A and D and are associated with the dashed red ray. The dashed blue raypath is associated with the virtual refraction ray that is excited by the virtual source (blue star) at C and terminates at B. Adapted from Hanafy and Schuster (2017).

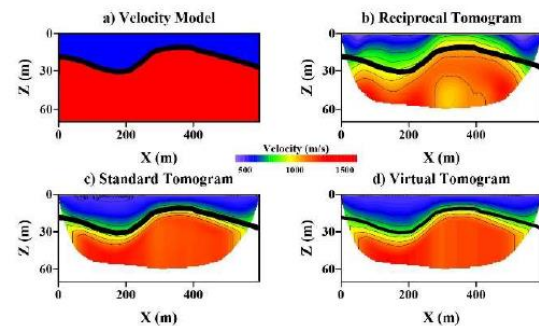


Figure 2. Two-layer model, b) reciprocal tomogram inverted from the 240 traveltimes in the two reciprocal shot gathers. c) standard tomogram inverted from traveltimes in 120 shot gathers, with a shot at each geophone location. d) Virtual tomogram inverted from O(14,000) virtual traveltimes created from 240 reciprocal traveltimes. There are 120 geophones.

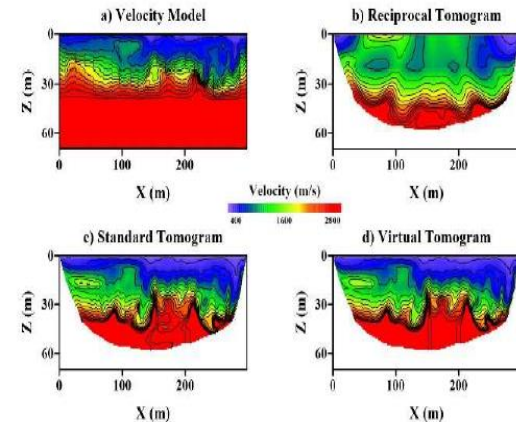
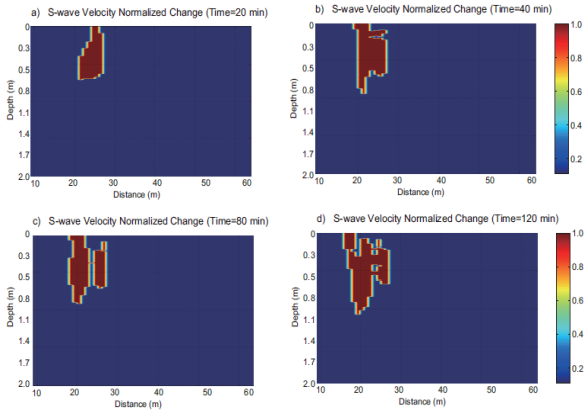
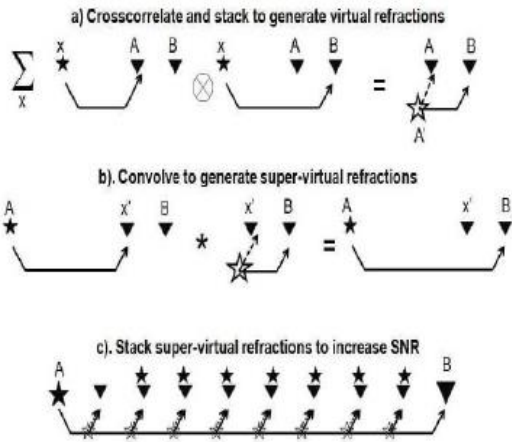


Figure 3. Similar to Figure 2 except for the complicated Aqaba velocity model in 3a).



**Figure 4.** S-velocity difference tomograms for different calendar times after >100 gallons of water was dumped on the surface over the offset range 18 m < x < 23 m.



**Figure 5.** The steps for creating 2D super-virtual refraction arrivals. a). Correlation of the recorded trace at **A** with that at **B** for a source at **x** to give the trace  $\Phi_x(\mathbf{A}, \mathbf{B}, t)$  with the virtual refraction arriving at the traveltimes denoted by  $\tau_{A'B} - \tau_{A'A}$ . This arrival time will be the same for all post-critical source positions, so stacking  $\sum_x \Phi_x(\mathbf{A}, \mathbf{B}, t)$  will enhance the SNR of the virtual refraction by  $\sqrt{N}$ , where  $N$  is the number of post-critical source-receiver pairs. b). Similar to that in a) except the virtual refraction traces are convolved with the actual refraction traces and stacked for different geophone positions to give the supervirtual traces in c). Supervirtual rays with the SNR of the supervirtual traces enhanced by  $\sqrt{N}$ . Here,  $N$  denotes the number of coincident source and receiver positions that are at post-critical offset. Illustration from Lu et al. (2014).

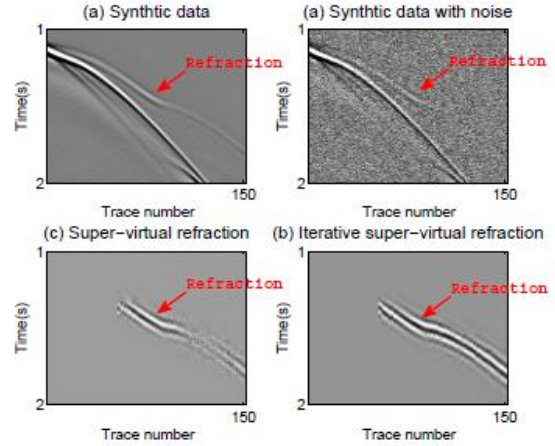


**Figure 6.** Far-offset traces for data with a) high SNR, b) low SNR, and c) traces after application of SVI to noisy data such as seen in b). The SNR of the SVI traces is further improved by applying iterative SVI to c) to give d).

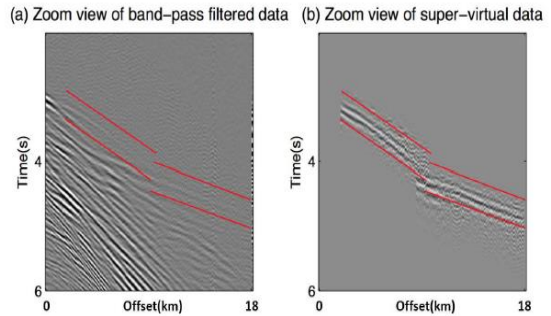


**Figure 7.** Far-offset traces of 3D marine data a) before and b) after application of 3D SVI to the data.